Probing photonic crystals on silicon-on-insulator with Ge/Si self-assembled islands as an internal source

X. Li, P. Boucaud,[a] and X. Checoury
Institut d'Électronique Fondamentale, UMR CNRS 8622, Bâtiment 220, Université Paris-Sud, 91405 Orsay, France

O. Kermarrec, Y. Campidelli, and D. Bensahel
STMicroelectronics, 850 rue Jean Monnet, 38926 Crolles Cedex, France

(Received 31 January 2005; accepted 2 December 2005; published online 24 January 2006)

We report the study of two-dimensional photonic crystals fabricated on silicon-on-insulator substrates. Ge/Si self-assembled islands are embedded as an active internal optical source inside the photonic crystals. We present a detailed analysis of photonic crystal microcavities and waveguides using the room-temperature Ge/Si island photoluminescence. The tunability of the microcavity resonant emission is demonstrated between 1.2 and 1.5 μm. We show that the microcavity photoluminescence is weakly dependent on the temperature. The polarized transmission properties of W1 single-line defect waveguides are investigated using the photoluminescence as an internal source. The transmission spectra are correlated to those given by two-dimensional finite-difference time-domain calculations. © *2006 American Institute of Physics*. [DOI: 10.1063/1.2163007]

I. INTRODUCTION

Two-dimensional photonic crystals are promising candidates for the development of silicon-based photonics. Both active and passive photonic devices can be realized by introducing a periodic variation of the permittivity in high index materials.[1,2] Two different approaches are usually proposed to realize semiconductor two-dimensional photonic crystal slabs with confinement of light in the vertical direction provided by index guiding. The first approach is the substrate approach where vertical waveguiding of light is obtained by a weak difference of the refractive index between the waveguide core and the cladding layers.[3] This approach that is widely used for III-V materials offers the advantage of a good thermal dissipation and is appropriate for electrical injection. It requires, however, some deep etching, and most of the light modes are found above the light line. The alternative approach is the so-called membrane approach where the vertical confinement of light is provided by a strong variation of the vertical index of refraction between the waveguide core and air.[4] Silicon-on-insulator (SOI) substrates are an ideal template to realize photonic crystals of this type with its upper crystalline layer acting as the waveguide core and the buried oxide layer as the cladding.[5] One advantage of the membranes or strongly confined waveguides on oxide is that a much larger number of modes are confined below the light line and that true lossless guided modes can exist for a large range of frequency and wave-vector values. Cavities with high-quality factors can be obtained with this approach. The probing of photonic crystal devices can be achieved either by an external source or using an internal source. The internal source technique has been largely investigated in the case of III-V materials.[6] For silicon-based materials, Ge/Si self-assembled islands with an emission covering the 1.2–1.6 μm spectral range can be used as internal sources to investigate the optical properties of the photonic crystals. Probing microcavities by the broad emission of the self-assembled nanostructures has been reported recently.[7,8]

In this work, we report a detailed analysis of photonic crystal microcavities and waveguides using the Ge island luminescence as an internal source. The tunability of the emission is demonstrated for both elongated cavities or hexagonal cavities. This tunability is achieved by changing the cavity size or changing the lattice periodicity. The optical response of the microcavities is investigated as a function of the temperature. We show that the emission weakly depends on the temperature and that the room-temperature optical recombination is only reduced by a factor of 2 as compared to the low-temperature (5 K) emission. The transmission of waveguides with a single defect line is finally investigated. Using an internal excitation inside the photonic crystal waveguide, i.e., without having to couple an external source to the waveguide modes,[9] we show that the W1 waveguide transmission can be probed in both TE (electric field parallel to the two-dimensional plane) and TM (magnetic field in plane) polarizations at room temperature. Resonant transmissions are observed in TM polarization for which no photonic band gap is present. These measurements are correlated to the photonic band diagram of the waveguide and to the transmission as calculated with a two-dimensional finite-difference time-domain calculation.

II. SAMPLE

The investigated sample was grown in an ASM chemical-vapor deposition reactor on a silicon-on-insulator substrate. It consists of a 40-nm-thick silicon layer above the oxide, a 50-nm-thick $p^+(10^{19}\ \mathrm{cm}^{-3})$-doped layer, a 20-nm-thick intrinsic silicon layer, a single Ge self-assembled layer embedded in a 80-nm-thick silicon matrix, and a 50-nm-thick $n^+(10^{19}\ \mathrm{cm}^{-3})$ layer. The buried oxide layer of the 200-

[a]Electronic mail: philippe.boucaud@ief.u-psud.fr

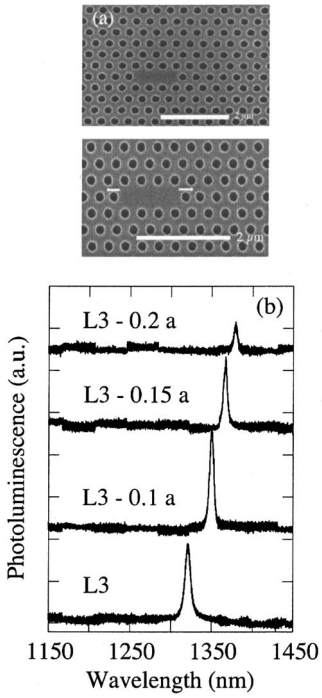

FIG. 1. (a) Scanning electron micrograph of an L3 microcavity (top image) and of an L3 microcavity with a lateral displacement of the edge holes of the cavity (0.15a, where a is the lattice periodicity). (b) Room-temperature photoluminescence of the L3 microcavity for different positions of the air holes at the edge of the cavity. The air holes are laterally displaced from bottom to top by a fraction of the lattice parameter a, as indicated on the figure.

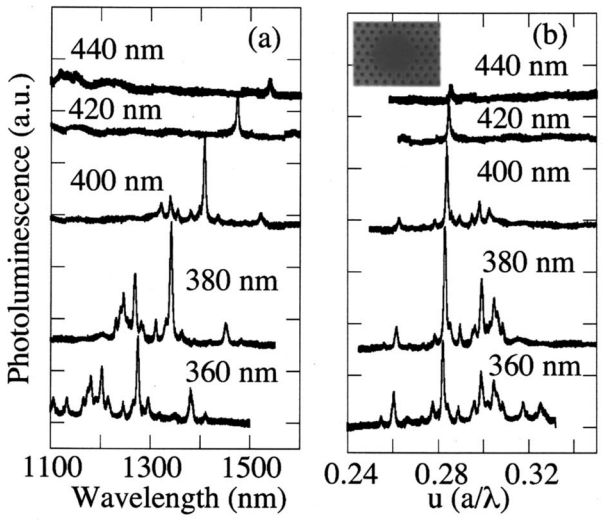

FIG. 2. Room-temperature photoluminescence of a hexagonal H3 microcavity for different lattice periods a of a triangular pattern. The figure on the left (a) shows the spectra as a function of the wavelength. The figure on the right (b) shows the same spectra as a function of the normalized frequency $u=a/\lambda$. The inset shows a scanning electron micrograph of the H3 microcavity.

mm-diam SOI substrate is 400 nm thick. The total thickness of the waveguide core including the doped layers and the Ge/Si island layer was 240 nm. The photonic crystals were realized by combining electron lithography and reactive ion etching. An oxide hard mask, 300 nm thick, was first deposited on top of the structure. The triangular lattice pattern was defined by electron lithography with a UV3 photoresist. The pattern was first transferred in the oxide hard mask using etching with CHF_3 gas and in a second step was transferred in the silicon matrix down to the buried oxide layer by reactive ion etching with SF_6+O_2 gases. The hole etch depth is thus 240 nm. The photonic crystals were probed with a microphotoluminescence setup using a continuous-wave 458 nm excitation delivered by an argon-ion laser. The incident excitation power was around 5 mW. For waveguide characterization, the island photoluminescence was excited from the surface at normal incidence, and the transmitted light was collected through the cleaved facet. The output of the waveguide was separated by 15 μm from the cleaved facet. The lattice periodicity a was varied between 360 and 440 nm.

III. RESULTS

A. Cavities

Figure 1(a) shows scanning electron micrographs of elongated cavities consisting of three missing air holes in a triangular pattern. The top image corresponds to the reference cavity while the bottom image corresponds to a cavity with a lateral displacement of the edge holes. The lattice periodicity a is 400 nm, and the hole radius is 0.35a. The lateral displacement of the edge holes shown on the bottom image is equal to 0.15a. A photonic band gap in TE polarization is calculated for this type of photonic crystal between 1120 and 1540 nm. Figure 1(b) shows the room-temperature photoluminescence spectra of cavities with variable hole displacements. A strong resonant emission is observed at room temperature close to 1.3 μm. This emission corresponds to one confined resonant mode of the microcavity for a normalized frequency $u=a/\lambda=0.3$, in good agreement with the calculated value using a plane-wave expansion ($u=0.297$). The quality factor of the emission is around 225 for the cavities with laterally displaced edge holes and 150 for the reference cavity. A weak emission is also observed close to 1480 nm ($u=0.27$ experimental, $u=0.271$ calculated). The emission can be tuned as a function of the lateral displacement of the edge air holes. It indicates that the resonant emission can be precisely controlled through the design of the cavity. We have not observed in this case a significant increase of the quality factor of the cavity as a function of the hole displacement.[10] We emphasize that the photonic crystals are not fabricated on a perforated membrane but on an oxide layer. Material absorption due to free-carrier absorption is also present because of the photogenerated carriers and of the doped layers in the structure.[11]

The tunability of the emission can also be achieved by varying the lattice periodicity. We have checked this tunability at room temperature for the case of photonic crystals on silicon-on-insulator containing Ge/Si self-assembled islands. Figure 2 shows the photoluminescence spectra of a hexagonal H3 microcavity for varying lattice periods. The spectra are depicted as a function of the wavelength in Fig. 2(a) and as a function of the normalized frequency $u(u=a/\lambda)$ in Fig. 2(b). The hole radius is proportional to a, $r/a=0.31$. The number of modes in the photonic band gap of the bulk structure, and, in particular, those coupled out of plane, are much

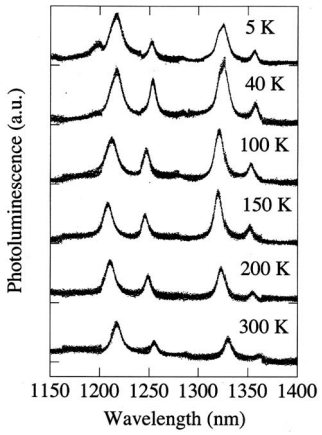

FIG. 3. Temperature dependence of the photoluminescence of a hexagonal H2 microcavity.

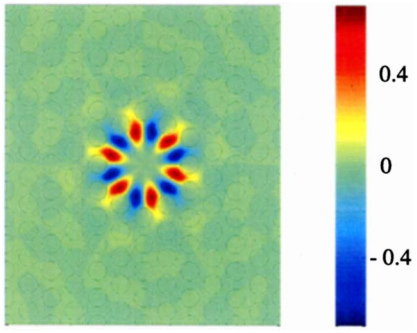

FIG. 4. (Color online) Spatial profile H_z of the H2 microcavity mode observed around 1220 nm ($u=0.355$). The black circles indicate the position of the air holes.

larger in these H3 cavities as compared to the previous elongated cavity. As seen, the emission can be easily tuned from 1.5 down to 1.2 μm. The main resonant peak observed for $u\sim0.282$ corresponds to a mode close to a whispering gallery mode. The out-of-plane coupling efficiency depends on the spectral overlap between the island luminescence and the coupling of the modes of the cavities. If we consider the emission as a function of the normalized frequency, the position of the resonances are observed, as expected, for a constant value of u. The small variation around a given value of u is likely attributed to the modal dispersion of the vertical waveguide and to the index variation as a function of the wavelength. We can observe that the amplitude of the photoluminescence decreases as the lattice periodicity increases, indicating that the spectral overlap with the island luminescence is not the only factor that governs the amplitude. The out-of-plane coupling depends on the spectral density for in-plane wave vectors lying between 0 and $2\pi n_{\text{oxide}}/\lambda$.[10] We have performed Fourier transforms of the electric field of the confined mode corresponding to $u=0.282$ for different lattice periodicities. As the lattice periodicity increases, the amplitude of the Fourier components in the zone center, i.e., in the leaky region, increases indicating that the quality factor of the cavity decreases. There is thus a decrease of the photoluminescence amplitude coupled out of plane for large lattice periodicities.

At room temperature, the photoluminescence amplitude exhibits a linear dependence as a function of the excitation power density. It indicates that the recombination process is limited by nonradiative recombination, even if the incident excitation intensity is large (a few milliwatt over a 2 μm spot diameter). Only a fraction of the incident light is absorbed in the thin silicon upper layer above the oxide. We have investigated the dependence of the photoluminescence amplitude as a function of the temperature. Figure 3 shows the temperature dependence in the case of a hexagonal H2 microcavity. At room temperature, the photoluminescence of this microcavity is characterized by four resonant modes which are associated with nondegenerate modes. The quality factor of these modes is around 150. The mode with the largest amplitude is close to a whispering gallery mode, as confirmed using a plane-wave calculation following the supercell approach. Figure 4 shows the mode profile of this resonant mode, as represented by its H_z component. The striking feature reported in Fig. 3 is that only a weak variation of the photoluminescence amplitude is observed as a function of the temperature. The amplitude decreases only by a factor of 2 from low temperature (5 K) to room temperature. The decrease is not uniform between the different resonant peaks. This variation is partly attributed to a variation of the position of the optical excitation by reference to the cavity center. A similar temperature dependence of the island photoluminescence was also observed in the unprocessed sample. It indicates that the nonradiative processes which govern the luminescence amplitude, either at the interface with the oxide or in the doped/undoped layers are weakly dependent on the temperature. A direct consequence of this feature is that the recombination is as efficient at room temperature as compared to low temperature in these silicon-on-insulator-based structures.

B. W1 waveguide

Key elements for integrated optics are waveguides with narrow widths. With photonic crystals, the light can be confined in a single-line defect. These single-line defects, i.e., consisting of one missing row of air holes, are usually referred to as W1 waveguides. They can be oriented along ΓK or ΓM directions. In the following, we demonstrate that the transmission of W1 photonic crystal waveguides on SOI can be probed with the Ge island luminescence as an internal source. The transmission spectra are interpreted from the waveguide dispersion as calculated with a plane-wave model and their transmission as obtained with two-dimensional finite-difference time-domain calculation.

Figure 5 shows a W1 waveguide transmission oriented along the ΓK direction in TM polarization [Fig. 5(a)] and TE polarization [Fig. 5(b)]. The lattice periodicity a of the structure is 440 nm, and the hole radius is $0.36a$. The waveguide is optically excited by the surface at different lateral positions, 10, 20, and 30 μm from the waveguide output. These distances correspond to $\sim$22, 45, and 68 lattice periods.The spot size is around 5 μm in diameter. The transmitted light is collected from the cleaved facet. The spectra are normalized with light transmitted in the same polarization and traveling through the unpatterned area. The amplitude is given in lin-

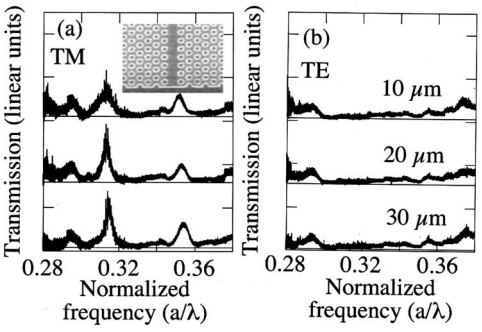

FIG. 5. Polarized transmission spectra in linear scale of a single defect W1 waveguide along ΓK direction as a function of the excitation position. The figure on the left (a) corresponds to the TM polarization, while the figure on the right (b) corresponds to the TE polarization. The vertical scale is identical for both figures. The position of the excitation of the luminescence by reference to the waveguide edge is indicated on the graph. The inset shows a scanning electron micrograph of the W1 waveguide. A reference base line has been added for each spectrum.

ear scale. As seen, the transmission is much larger in TM polarization with enhanced transmission resonances for $u=0.31$ and $u=0.35$. The amplitude of the transmitted light does not significantly change as a function of the position, thus indicating that the losses are not significant on this length scale. Note that a slight modification of pump injection in the waveguide can modify the amplitude of the transmission. As explained below, the observed resonances correspond to band-edge modes. In TE polarization, the transmission amplitude is much smaller as compared to that in TM polarization. In both cases, the transmission amplitude depends on the coupling efficiency of the photoluminescence to the waveguide modes. The transmission is nearly constant for normalized frequencies varying between 0.3 and 0.36. A weak increase of transmission is observed for $u=0.29$ and 0.37. The dynamics of the measurement in this spectral range is, however, not sufficient to estimate accurately the propagation losses and, in particular, the diffraction losses for the TE polarization.[12]

The waveguide band diagram was calculated with a two-dimensional plane-wave model using a supercell approach. The effective index of the fundamental mode vertically confined was introduced in the calculation to account for planar confinement in the vertical direction ($n_{\mathrm{eff}}=2.9$ and $n_{\mathrm{eff}}=2.05$ for TE and TM polarizations, respectively). An air filling factor $f=2\pi r^2/a^2\sqrt{3}=47\%$ consistent with scanning electron micrograph measurements was considered. Both index-guided modes and photonic crystal modes appear in the band diagram. Figure 6 shows the W1 waveguide band diagram in TE polarization [Fig. 6(a)] and TM polarization [Fig. 6(b)]. The light lines corresponding to air and cladding are highlighted as dashed lines. Below the light line, the modes are truly guided whereas above the light line the modes are leaky and suffer radiation losses due to out-of-plane diffraction. At the edge of the Brillouin zone, the first two modes ($u=0.264$ and $u=0.277$) correspond to the fundamental mode and are clearly below the oxide light line. These modes are well confined within the waveguide. The mode at $u\sim0.34$ is also well confined inside the waveguide. This mode is very close to to the oxide light line. Its position

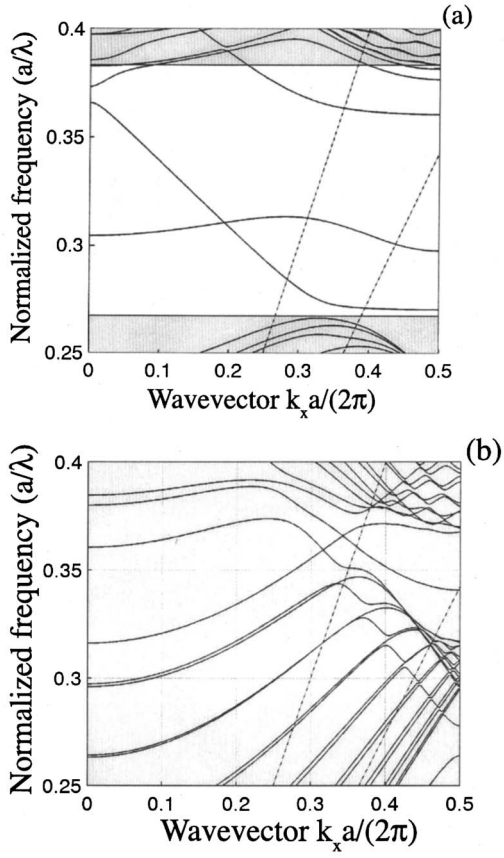

FIG. 6. Calculated band diagram of the W1 waveguide for TE [top (a)] and TM [bottom (b)] polarizations as obtained with a plane-wave calculation. The air and oxide light lines are indicated as dashed lines, respectively. For TE polarization, the spectral region with no band gap for the bulk photonic crystal has been shaded.

above or below the oxide light line depends on the exact value taken in the calculation for the effective index and on the value of the oxide refractive index ($n=1.46$ in the present case). In TE polarization, the photonic band gap of the triangular lattice extends from $u=0.267$ to $u=0.3825$. For the W1 waveguide oriented along ΓK direction, a stop band is expected at the edge of the Brillouin zone between $u=0.20$ and $u=0.21$ and at the zone center ($u=0.36-0.365$) corresponding to the stop band of the fundamental mode. A ministop band is also expected between $u=0.26$ and 0.265. The spectral range between 0.265 and 0.36 corresponds to the transmission window of the fundamental mode inside the photonic band gap. In TM polarization, no photonic band gap is obtained, as expected from the air filling factor of the photonic crystal. The stop band of the fundamental mode at the edge of the Brillouin zone is calculated to occur for u varying between 0.265 and 0.28.

The transmission properties of the waveguides will depend on the coupling of the light to the different modes as well as on their dispersion and group velocity. The excitation occurs inside the waveguide, i.e., there is no coupling from an external source outside the waveguide to the fundamental mode of the waveguide. No mode mismatch between the photonic crystal waveguide and the slab waveguide is thus present in this case. Additionally, no external stripe waveguide is required to inject light into the photonic crystal

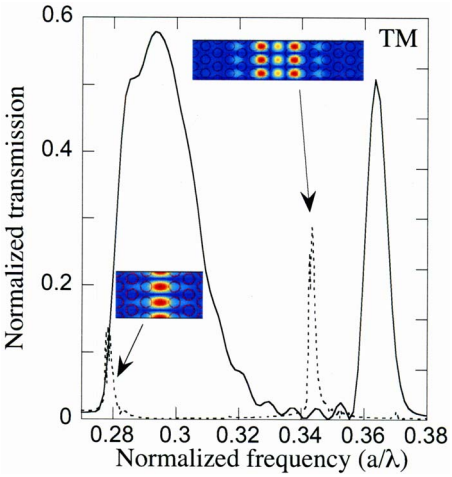

FIG. 7. (Color online) Finite-difference time-domain calculation of the normalized transmission of a W1 waveguide in TM polarization (full line). Finite-difference time-domain calculation of the transmission of a W1 waveguide in TM polarization, as measured from the tail of the pulsed excitation exiting from the waveguide (dashed line). The corresponding spatial profiles of the associated modes at the edge of the Brillouin zone are indicated on the figure. The amplitude of the dashed curve is not normalized.

waveguide. The transmission spectra can thus be different from those usually measured with III-V photonic crystal waveguides.[13] We have performed finite-difference time-domain (FDTD) calculation on this system by solving time-dependent Maxwell equations. The same effective indexes were considered in TE and TM polarizations as for the plane-wave calculations. An internal point pulsed source was inserted in the waveguide with a broad emission ($\Delta u = \pm 0.1$), and we have recorded the normalized transmission as a function of the normalized frequency.[14] No losses were introduced in the calculation. The transmission spectra of the W1 waveguide in TM polarization is shown in Fig. 7. In FDTD, a dip in transmission is calculated between $u=0.26$ and 0.27, corresponding to the stop band of the fundamental mode at the edge of the Brillouin zone. Two resonances are observed for $u=0.3$ and $u=0.36$. The resonance at $u=0.36$ is in satisfying agreement with the observed experimental value ($u=0.35$). Around $u=0.3$, a double resonance is experimentally observed, while a broad transmission resonance is calculated. In the FDTD calculation, only a very weak fraction of the energy is coupled to the band-edge Bloch modes with a low group velocity. The contribution of these low group velocity modes is not dominant as compared to the main flow of energy. We also present in Fig. 7 the calculated transmission of the waveguide as obtained from the tail of the pulsed excitation exiting from the waveguide (dashed line). The resonances correspond to the band-edge Bloch modes with a spatial profile well localized inside the waveguide. The difference between the calculated and measured values of normalized frequencies at resonance is partly attributed to the change of the effective index as a function of the wavelength which is not taken into account in the calculation. We emphasize that the experimental continuous excitation differs from the pulsed excitation used in FDTD. Note that symmetry breaking which results in mode coupling can also contribute to the discrepancy between experiments and calculation and that the spectral selection resulting from the experimental setup might also contribute to the difference between near-field mode calculation and spectra resulting from far-field collected modes. In TE polarization (not shown), the calculated transmission as obtained by FDTD is nearly constant between $u=0.27$ and $u=0.35$. This feature is associated with the uniform transmission of the fundamental guided mode. Different sets of parameters should be used to design waveguides with a stop band that overlaps significantly with the Ge/Si island emission in order to analyze band-edge features.

IV. CONCLUSION

In conclusion, we have provided a detailed analysis of photonic crystal structures fabricated on silicon-on-insulator substrates by using the room temperature photoluminescence of Ge/Si self-assembled islands as an internal source. The tunability of out-of-plane coupled emission in the spectral range between 1.2 and 1.5 μm was demonstrated either for elongated cavities or hexagonal cavities. The tunability is achieved either by shifting the air holes to the edge of the cavities or by changing the photonic crystal lattice periodicity. We have shown that the room-temperature emission collected from cavities is only reduced by a factor of 2 in amplitude as compared to the low-temperature emission. The study of a single defect-line waveguide was finally reported. The transmission can be probed both in TM and TE polarizations with an optical excitation inside the waveguide. The spectral dependence of the transmission was correlated to the photonic band diagram of the waveguide and to the transmission as calculated using a finite-difference time-domain formalism. Resonant enhanced transmissions in TM polarization were observed.

ACKNOWLEDGMENT

This work was supported by the Nano2008 program of the French Ministry of Industry.

[1] E. Yablonovitch, Phys. Rev. Lett. **58**, 2059 (1987).
[2] S. John, Phys. Rev. Lett. **58**, 2486 (1987).
[3] T. D. Happ, M. Kamp, A. Forchel, J. L. Getner, and L. Goldstein, Appl. Phys. Lett. **82**, 4 (2003).
[4] *International Workshop of Electromagnetic Structures (PECS III), St Andrews, UK, 2001*, edited by T. Krauss [Opt. Quantum Electron. **34**, 1 (2002)], and references therein.
[5] M. Notomi, A. Shinya, K. Yamada, J. Takahashi, C. Takahashi, and I. Yokohama, IEEE J. Quantum Electron. **38**, 736 (2002).
[6] H. Benisty *et al.*, J. Lightwave Technol. **17**, 2063 (1999).
[7] S. David, M. El kurdi, P. Boucaud, A. Chelnokov, V. Le Thanh, D. Bouchier, and J.-M. Lourtioz Appl. Phys. Lett. **83**, 2509 (2003).
[8] M. El Kurdi, S. David, P. Boucaud, C. Kammerer, X. Li, V. Le Thanh, S. Sauvage, and J.-M. Lourtioz, J. Appl. Phys. **96**, 997 (2004).
[9] D. Labilloy *et al.*, Phys. Rev. Lett. **79**, 4147 (1997).
[10] Y. Akahane, T. Asano, B-S. Song, and S. Noda, Nature (London) **425**, 944 (2003).
[11] I. Alvaro-Rodriguez and E. Yablonovitch, J. Appl. Phys. **92**, 6399 (2002).
[12] L. C. Andreani and M. Agio, Appl. Phys. Lett. **82**, 2011 (2003)
[13] S. Olivier *et al.*, Appl. Phys. Lett. **79**, 2514 (2001).
[14] M. Qiu, K. Azizi, A. Karlsson, M. Swillo, and B. Jaskorzynska, Phys. Rev. B **64**, 155113 (2004).